NUMERICAL MODELLING OF SHEET-FLOW TRANSPORT UNDER WAVE AND CURRENT

Abbas Yeganeh-Bakhtiary[1], Hotoshi Gotoh[2], and Tetsuo Sakai[2]

[1] Research Center for Disaster Environment, Disaster Prevention Research Inst., Kyoto University, Uji, Kyoto 611-0011, Japan
[2] Department of Civil Engineering, Kyoto University, Kyoto 606-8501, Japan

Abstract: An Euler-Lagrange two-phase flow model is presented for simulation sheet-flow transport under wave and current. The flow is computed by solving the Reynolds Averaged Navier-Stokes equation in conjunction with the k-ε turbulence model for turbulence closure. The sediment transport is introduced as a motion of granular media under the action of unsteady flow from the Lagragian point of view. In other word, motion of every single particle is numerically traced with Movable Bed Simulator (MBS) code based on the Distinct Element Method (DEM), in which the frequent interparticle collision of the moving particles during the sheet-flow transport is sophisticatedly taken into account. The particle diameter effect on time-dependent developing process of sheet-flow transport is investigated, by using three different diameter sizes of sediment. The influence of an imposed current on oscillatory sheet-flow transport is also investigated. It is concluded that the sediment transport rate increases due to the relaxation process related to the time-lag between flow velocity and sediment motion.

Key Words: wave, current, oscillatory flow, sheet-flow, interparticle collision, MBS, DEM

1. INTRODUCTION

Severe beach topography change often takes place during stormy wave condition when sheet-flow mode of transport is predominant. Sheet-flow mode is conventionally referred to the bed-load transport at high bottom shear stress, while sediment grains move in a layer very close to bed with a thickness of several times of a grain diameter.

Sheet-flow transport is a hyper-concentrated fluid-sediment mixture induced by periodically unsteady flow motion, the hydrodynamics of transport, therefore, is very complex, and its knowledge is still poor. On the other hand, numerical simulation, as the most viable techniques, provides more insightful knowledge on the hydrodynamics of transport. Asano (1990) proposed a numerical model for simulation of oscillatory sheet-flow in the framework of two-phase flow. Asano's model is constructed based on Euler-Euler coupling of the governing

equations of solid and fluid phases, and the result of his model agrees quite well with the experimental data of Horikawa *et al.* (1982). However, the frequent interparticle collision, which is the main characteristics of sheet-flow motion, is neglected in the Euler-Euler coupling model.

Gotoh and Sakai (1997) performed a pioneer work on the simulation of sheet-flow transport from the viewpoint of granular material dynamics. In their model, the sediment motion as well as the frequent interparticle collision of moving particles are simulated with using a Lagrangian method, based on the *Distinct Element Method* of Cundall and Strack (1979). Later Yeganeh *et al.* (2000) developed an Euler-Lagrange two-phase flow model for simulation of oscillatory sheet-flow motion. In this model the flow is computed with Reynolds Averaged Navier-Stokes equation in conjunction with the k-ε turbulence model for turbulence closure.

In this study, the pervious model of Yeganeh *et al.* (2000) is upgraded to simulate the sheet-flow transport under the action of wave and current. The flow field is described with oscillatory flow, which approximates wave driven motion, combined with a steady unidirectional current. The sediment phase is simulated with the aid of the Movable Bed Simulator (MBS) code of Gotoh and Sakai (1997), in which the sediment particles response to flow acceleration and deceleration process is traced form the Lagrangian point of view. Furthermore, the particle diameter effect on the time-dependent developing process of sheet-flow transport is considered by using three different diameter size of sediment.

2. MATHEMATICAL FORMULATION

In this section, the governing equations of the flow field and sediment motion will be summarized.

2.1 Fluid-phase formulation

The governing equations of the fluid phase is described with a vertically two-dimensional k-ε turbulence model as follows:

$$\frac{\partial U}{\partial x}+\frac{\partial V}{\partial y}=0 \tag{1}$$

$$\frac{\partial U}{\partial t}+U\frac{\partial U}{\partial x}+V\frac{\partial U}{\partial y}= -\frac{1}{\rho}\frac{\partial P}{\partial x}+\frac{\partial}{\partial x}\left(2\Gamma\frac{\partial U}{\partial x}\right)+\frac{\partial}{\partial y}\left[\Gamma\left(\frac{\partial U}{\partial y}+\frac{\partial V}{\partial x}\right)\right] \tag{2}$$

$$\frac{\partial V}{\partial t}+U\frac{\partial V}{\partial x}+V\frac{\partial V}{\partial y}=-g-\frac{1}{\rho}\frac{\partial P}{\partial y} +\frac{\partial}{\partial x}\left[\Gamma\left(\frac{\partial U}{\partial y}+\frac{\partial V}{\partial x}\right)\right]+\frac{\partial}{\partial y}\left(2\Gamma\frac{\partial V}{\partial y}\right) \tag{3}$$

$$\frac{\partial k}{\partial t}+U\frac{\partial k}{\partial x}+V\frac{\partial k}{\partial y}=\frac{\partial}{\partial x}\left[\left(\nu+\frac{\nu_t}{\sigma_k}\right)\frac{\partial k}{\partial x}\right] +\frac{\partial}{\partial y}\left[\left(\nu+\frac{\nu_t}{\sigma_k}\right)\frac{\partial k}{\partial y}\right]+P_r-\varepsilon \tag{4}$$

$$\frac{\partial \varepsilon}{\partial t}+U\frac{\partial \varepsilon}{\partial x}+V\frac{\partial \varepsilon}{\partial y}= \frac{\partial}{\partial x}\left[\left(\nu+\frac{\nu_t}{\sigma_\varepsilon}\right)\frac{\partial \varepsilon}{\partial x}\right]+\frac{\partial}{\partial y}\left[\left(\nu+\frac{\nu_t}{\sigma_\varepsilon}\right)\frac{\partial \varepsilon}{\partial y}\right] +\frac{\varepsilon}{k}\left(C_{1\varepsilon}P_r-C_{2\varepsilon}\varepsilon\right) \tag{5}$$

$$P_r=\nu_t\left[2\left(\frac{\partial U}{\partial x}\right)^2+2\left(\frac{\partial V}{\partial y}\right)^2+\left(\frac{\partial U}{\partial x}+\frac{\partial V}{\partial y}\right)^2\right] \tag{6}$$

$$\Gamma=\nu+\nu_t\ ;\ \nu_t=C_\mu\frac{k^2}{\varepsilon} \tag{7}$$

in which U, V = components of mean-flow ve-

locity in x, y direction; x, y = streamwise and upward-vertical coordinates; ρ = mass density of water; P = pressure; Γ = effective viscosity; g = acceleration of gravity; k = turbulent kinetic energy; ν = kinematic viscosity; ν_t = kinematic eddy viscosity; P_r = production of turbulent kinetic energy due to shear stress; and ε = dissipation of turbulent kinetic energy. The recommended values for the constants in the k-ε turbulence model are as follows: C_μ = 0.09; σ_k =1.0; σ_ε =1.3; $C_{1\varepsilon}$ =1.44; and $C_{2\varepsilon}$ =1.92.

2.2 Sediment phase model

The sediment grains are modeled by spherical particles with the uniform diameter, and tracked in a vertically two-dimensional plane. At every contacting point of particles, a spring-dashpot system is introduced to express the particle/ particle interaction. The equations of motion of the i_{th} particle in the vertically two-dimensional coordinate are as follows:

$$\rho\left(\frac{\rho_s}{\rho}+C_M\right)A_3 d^3\frac{du_{Pi}}{dt} = \sum_j\left[f_n\cos\alpha_{ij}+f_s\sin\alpha_{ij}\right]_j + \frac{\rho}{2}A_2 d^2 C_D\left|\mathbf{U}-\mathbf{u}_{pi}\right|\left(U-\mathrm{u}_{Pi}\right) \tag{8}$$

$$\rho\left(\frac{\rho_s}{\rho}+C_M\right)A_3 d^3\frac{dv_{Pi}}{dt} = \sum_j\left[-f_n\sin\alpha_{ij}+f_s\cos\alpha_{ij}\right]_j - \rho\left(\frac{\rho_s}{\rho}-1\right)A_3 d^3 g + \frac{\rho}{2}A_2 d^2 C_D\left|\mathbf{U}-\mathbf{u}_{pi}\right|\left(V-\mathrm{v}_{Pi}\right) \tag{9}$$

$$\left|\mathbf{U}-\mathbf{u}_{pi}\right| = \sqrt{\left(U-\mathrm{u}_{Pi}\right)^2+\left(V-\mathrm{v}_{Pi}\right)^2} \tag{10}$$

$$\frac{\pi d^4}{32}\frac{d\omega_{Pi}}{dt} = \frac{d}{2}\cdot\sum_j\left(f_s\right)_j \tag{11}$$

in which ρ_s = mass density of sediment particle; C_M = added mass coefficient (= 0.5); A_2, A_3 = two- and three-dimensional geometrical coefficients; d = particle diameter; u_{pi}, v_{pi} = velocity components of particle in x and y directions; f_n, f_s = normal and tangential forces acting between i_{th} and j_{th} particles on the n-s local coordinate system (see Fig.1); C_D = drag coefficient (= 0.4); α_{ij} = contacting angle between i_{th} and j_{th} particles; $\mathbf{U}$, $\mathbf{u}_{pi}$ = velocity vector of fluid and particle, respectively; and $\omega_{P\,i}$ = rotational angle of the i_{th} particle.

In the case of the uniform-diameter particles, the assessment of contacting particle is simply formulated as

$$\sqrt{\left(x_i-x_j\right)^2+\left(y_i-y_j\right)^2} \le \gamma d \tag{12}$$

in which (x_i, x_j), (y_i, y_j) = coordinates of the centroid of i_{th} and j_{th} grains; and γ = constant around 1.0.

Between each contacting particles the spring-dashpot system should be activated in both normal and tangential directions of the local coordinate, as shown in Fig.1. The acting force between two adjacent contacting particles i and j can be estimated by

$$f_n(t) = e_n(t)+d_n(t) \tag{13}$$

$$e_n(t) = e_n(t-\Delta t)+k_n\Delta\varsigma_n \tag{14}$$

$$d_n(t) = \eta_n\,\Delta\varsigma_n/\Delta t \tag{15}$$

$$f_s(t) = e_s(t)+d_s(t) \tag{16}$$

$$e_s(t) = e_s(t-\Delta t)+k_s\Delta\xi_s \tag{17}$$

$$d_s(t) = \eta_s\,\Delta\xi_s/\Delta t \tag{18}$$

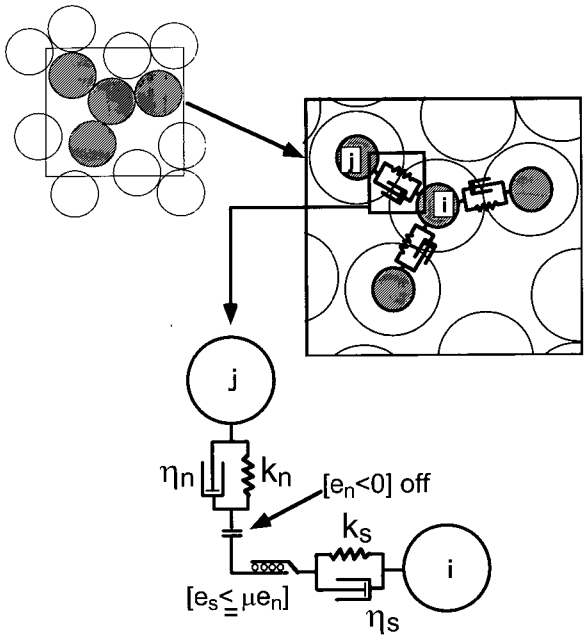

Fig.1. Multiparticle collision and interaction system between contacting grains (Gotoh and Sakai, 1997)

in which e_n, e_s = forces working on springs; d_n, d_s = forces acting on dashpots; $\Delta\zeta_n$, $\Delta\xi_s$ = displacement of particles during a time step Δt; k_n, k_s = spring constants; and η_n, η_s = damping coefficients.

Since non-cohesive particle is treated herein, the joint with no resistance to tensile force is assumed in normal direction; whereas, in tangential direction the frictional force activates. This characteristic of the contacting joint is featured with the following equations, in which joint slips at the limit of shear stress is applied in the tangential direction:

$$f_n(t) = f_s(t) = 0 \quad when \quad e_n(t) < 0 \tag{19}$$

$$f_n(t) = \mu SIGN[e_n(t), e_s(t)] \quad when \quad e_s(t) < \mu e_n(t) \tag{20}$$

$$SIGN[a,b] = \begin{cases} +|a| & when \quad b \geq 0 \\ -|a| & when \quad b < 0 \end{cases} \tag{21}$$

in which μ = friction coefficient (= 0.570).

2.3 Tuning of model parameter

According to Cundall and Strack (1979), to guarantee the stability of numerical schemes of DEM calculation, the time step Δt should be taken as a fraction of critical time step or Δt_c. Δt can be estimated on the basis of the Δt_c of the single mass-spring system with a single degree of freedom as

$$\Delta t = \Delta t_c / 20 \quad ; \quad \Delta t_c = 2\pi\sqrt{m/2k_n} \tag{22}$$

in which m = mass of single particle.

In this study the time step value is adopted as Δt=0.0002s; thus, k_n is estimated by Eq. 22.

From the theory of elasticity k_s is given by

$$k_s = \frac{k_n}{2(1+\nu_p)} \tag{23}$$

in which ν_p = Poisson's ratio (= 0.3).

The damping coefficients are estimated from the following critical damping conditions of Voigt model:

$$\eta_n = \alpha_{cn} 2\sqrt{mk_n} \; ; \quad \eta_n = \frac{\eta_n}{2(1+\nu_p)} \tag{24}$$

in which α_{cn} = 1.0.

2.4 Initial and boundary condition

Both sides of calculating domain are periodic to save the calculation time. At the bottom, the wall function is implemented as boundary condition, namely the logarithmic law holds between the wall and its adjacent grid point. For the proper fitting of logarithmic velocity distribution, the theoretical bed level is set below the average height of bed surface (see Yeganeh (1999) for more details). The boundary condition for streamwise velocity at the grid point ($y = y_p$) near bottom vicinity is expressed as follows:

$$\frac{U(y_p,t)}{u_*} = \frac{1}{\kappa}\ln(30.1\frac{y_p}{r_b}) \tag{25}$$

in which κ = von-Kármán constant (= 0.41); r_b = bed roughness; and u_* = shear velocity.

An additional assumption of the local equilibrium between generation and dissipation of turbulent energy is made at the grid points near the bottom wall, hence k and ε at the first grid are calculated respectively by

$$k = \frac{u_*^2}{\sqrt{C_\mu}} \quad ; \quad \varepsilon = \frac{u_*^3}{\kappa y_p} \tag{26}$$

Before the main calculation, packing calculation is executed to determine the initial location of particles. In the packing procedure, particles are initially arranged with leaving a 0.001cm gap between each adjacent particle. During the packing process, velocity of particles is monitored to assess the convergence of packing calculation. After packing calculation, the main calculation is performed to trace the motion of sediments under the action of unsteady fluid flow. The main calculation consists of two loops: the outer-loop for the flow calculation and the inner-loop for the MBS calculation. The outer-loop, which equals to one cycle of oscillatory flow motion, totally takes 4 seconds. In the inner-loop the flow information is feed-backed to the MBS code, and the sediments motion is monitored during the unsteady fluid action. The calculation is continuously performed until it reaches to a fully developed cyclic behavior of sheet-flow transport.

Table 1. Hydraulic condition of numerical experiments

Numerical experiments		d(mm)	U_c/U_{max}	f	τ_*
case1	# 1-1	1	0.1	0.035	1.3
	# 2-1	5	0.1	0.074	0.55
case2	# 2-2	5	0.3	0.068	0.71
	# 2-3	5	0.5	0.064	0.88
case3	# 3-1	10	0.1	0.105	0.39

The flow depth is 15.0 cm in this numerical experiment, and the maximum free stream flow velocity, U_{max}, reaches to 100.0 cm/s. The current velocity, U_c, is adopted as 10, 30, and 50 cm/s. The test particles are consisted of 0.1, 0.5, 1.0 cm in diameter and 2.65 in specific gravity, respectively. In the calculating domain, totally 50 particles are randomly placed in 10 layers: there are 5 particles in each layer, (see Yeganeh (1999) for more details). Table 1 shows the hydraulic condition of the numerical experiments.

3. DISCUSSION AND RESULTS

3.1 Flow velocity

Figure 2 depicts time series of velocity distribution for the combined oscillatory flow and current, case 2-3 with U_c/U_{max} = 0.5. The ratio of U_c/U_{max} is considered as the key parameter to describe the effect of an imposed current on oscillatory flow field. Numbers on the figure refer to the phases of flow's free stream velocity.

Fig.2 indicates that the characteristics of oscillatory flow velocity will be affected, provided that a strong current superimposed on oscillatory flow field. As far as the imposed current acts in the direction of oscillatory motion (in our numerical experiments at acceleration phases), the velocity overshoot near bed, which is the typical feature of the oscillatory boundary layer, disappears. While the imposed current acts in the direction against to oscillatory flow, the velocity overshoot near bed becomes very significant. It is apparently shows that imposing of a strong current on a oscillatory flow field has the nature to damp wave motion near bed, since it alternatively adds to and subtracts from the free stream velocity, $U_{max}\ sin(\omega t)$.

3.2 Sheet-flow transport rate

Time variation (every $\pi/32$ phase differences) of the nondimensional sediment transport rate q_{b*}, is depicted in Fig.3, cases 1-1, 2-1 and 3-1. The transport rate is estimated after 10 cycles of

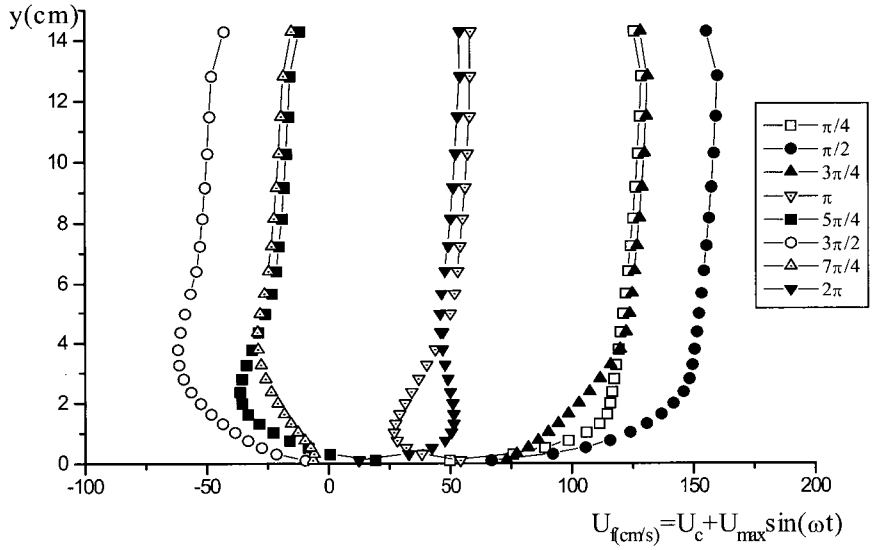

Fig.2. Time series of velocity of the oscillatory flow and current

calculation or 40 seconds when total sheet-flow transport rate is almost at the fully developed condition. q_{b*} is defined as follows:

$$q_{b*} = \frac{q_b}{\sqrt{(\rho_s/\rho - 1)gd^3}} \tag{27}$$

in which q_b = sediment transport rate.

The transport rate shows rather simple harmonic behavior, but it retards from the free stream flow velocity. The figure also describes effects of particle diameter on the time-lag between sheet-flow transport and free stream velocity. It is apparent that the time-lag increases with the particle diameter. For example, in the case of the largest particle (d =1.0cm) the time-lag reaches to almost $\pi/4$; while, in the case of the finest one, it confines to almost $\pi/32$ or less. On the other hand, the same tendency cannot be clearly detected for maximum transport rate. It appears that the nondimensional transport rate clearly depends on the particle diameter, hence the larger the particle is, the less rate of transport is induced.

3.3 Current effect on sheet-flow transport

Figure 4(a) illustrates the influence of an imposed current on the nondimensional transport rate during the time-dependent process of sheet-flow transport, cases 2-1, 2-2 and 2-3. When the imposed current is in the same direction as the flow mo tion, the transport rate increases with the increase of U_c/U_{max}. However, the sheet-flow transport rate decreases markedly when the current flow acts against the oscillatory flow motion. The discrepancy in transport profiles at the deceleration phases may be attributed to the interparticle collision of moving particles due to flow unsteadiness in combined wave-current motion. It can be concluded from the figure that superposition of a current generally increases the sheet-flow transport rate.

Figure 4(b) depicts the streamwise velocity of moving particles at y/d = 0.5. The streamwise particle's velocity is averaged at the final cycle of calculation. The profile of particle's velocity has a general trend that particle motion is retarded from the flow's free stream velocity. This

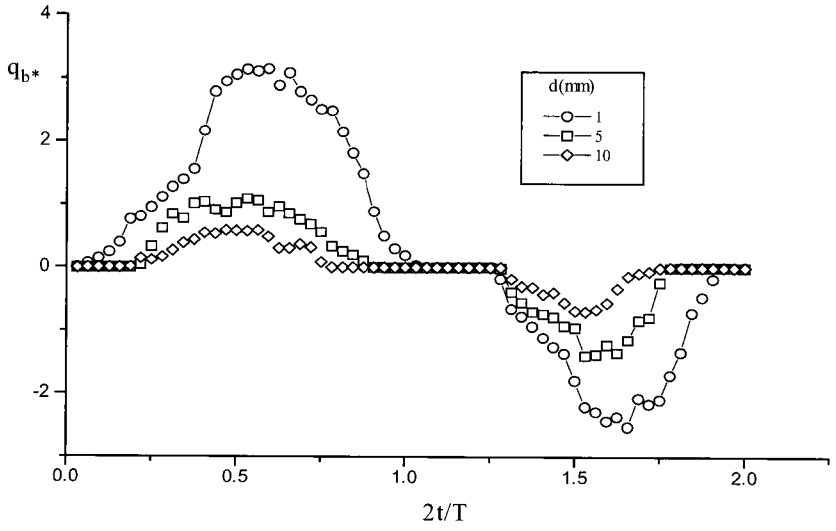

Fig.3. Non-dimensional sheet-flow transport rate

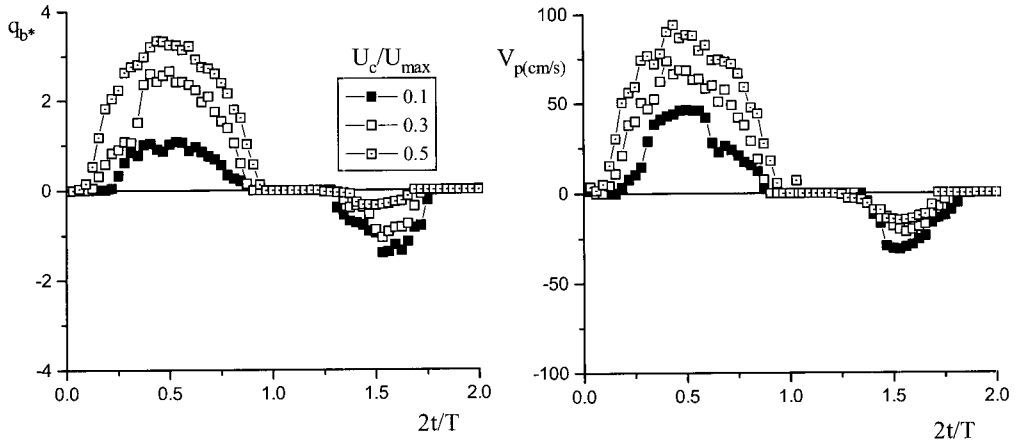

(a) Non-dimensional transport rate (b) Grain's mean-velocity

Fig.4. Current effect on sheet-flow transport

trend can be readily observed in the figure 4.a for the nondimensional transport rate, too. When the current acts against oscillatory flow motion, however, the retardate time between moving particles and flow's free stream velocity increases with the increase of U_c/U_{max}. Therefore, it is evident that, at the deceleration phase, moving particles do not respond keenly to oscillatory flow since the driving forces is reduced by the acting current. Instead moving particles undergoes rather a moving-grain induced process, which is mainly governed by the interparticle collision system and termed as the sediment relaxation process, (see Yeganeh *et al.* (2000) for more details). It initiates a time-lag between sediment motion and flow's free stream velocity.

On the other hand, the time-lag between free stream velocity and moving particles is reduced at the acceleration phase when the imposed current act in the same direction of the oscillatory flow. The time-lag effect induces skewness at the decelerated phases in Fig.4: the rising limb of the profile shows an upward concave shape, while the falling limb tends to an upward convex one.

It may be concluded from the present result that superposition of a current on wave motion may generally increases the sheet-flow transport rate. Furthermore, as the current component of combined wave and current flow increases, the net transport will be increased remarkably.

3.4 Half-cycled averaged transport rate

Fig.5 shows the averaged nondimensional sheet-flow transport rate as a function of the nondimensional bottom shear stress, τ_*. In connection with oscillatory sheet flow transport, τ_* is generally defined in terms of bottom-shear-stress amplitude, τ_{*max} as:

$$\tau_{*max} = \frac{f U_{fmax}^2}{2(\rho_s/\rho - 1)gd} \quad ; \quad U_{fmax} = U_c + U_{max} \tag{28}$$

in which f = friction factor and U_{fmax} = maximum flow velocity. In this study the bed roughness value is adopted as d, and the oscillatory friction factor is estimated based on Tanaka's

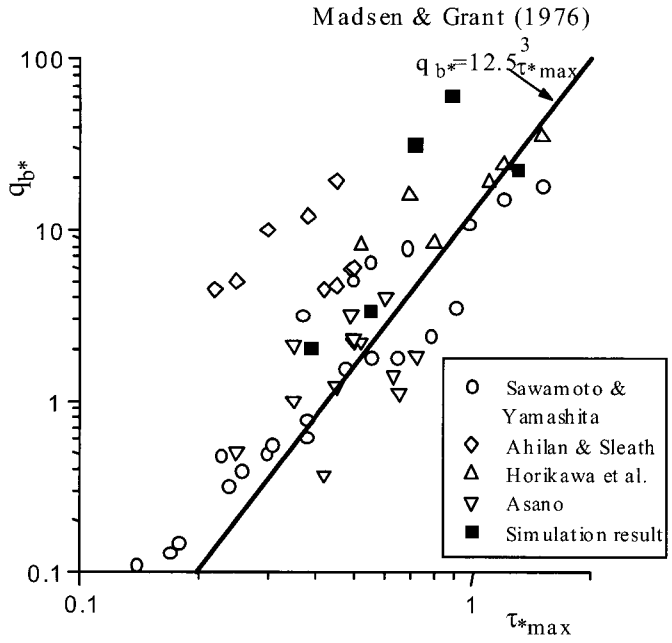

Fig.5. Net sheet-flow transport rate

formula (1993) as follows:

$$f = \exp\left[-7.53 + 8.07\left(\frac{U_{max}}{\omega z_0}\right)^{-0.1}\right] \qquad (29)$$

in which ω= radian frequency and z_0 = zero-intercept level of logarithmic velocity profile(= d).

The sheet-flow transport rate that estimated by the simulation model is found to yield a good agreement with the experimental data sets. However, the formula of Madsen and Grant (1976) is not able to represent the sheet-flow transport rate very well if the influence of superposition current is significant.

4. CONCLUSIVE REMARKS

In this study a numerical model for simulating sheet-flow transport under wave and current is presented. The simulation result confirms that the moving grains induce rather a complicated relaxation process at sheet-flow mode, which depends on the grain's diameter. The larger grain is, the longer time-lag is expected.

The profile of nondimensional transport rate as well as time dependent velocity of moving grains present a skewness in which the rising limb of the profile shows an upward concave shape, whereas the falling limb of it tends to an upward convex one. This skewness increases in the case of combine wave and current flow. Because at the phases when coexisting current acts in the opposite direction of oscillatory flow, the time-lag between tmoving grains and free stream velocity increases with increase of the ratio U_c/U_{max}, due to the inertia effect arises from the interparticle collision.

It is concluded from the present result that the superposition of a current on oscillatory flow motion generally increases the sheet-flow

transport rate. As the current component of combined wave and current flow becomes increased, the sheet-flow transport rate will be increased remarkably, and the conventional formula may not represent it accurately.

ACKNOWLEDGEMENT

The authors wish to express their gratitude to Dr. Toshiyuki Asano, Professor at Department of Ocean and Civil Engineering, Kagoshima University, for his constructive suggestion on the building of the oscillatory flow part of model. The first author expresses his sincere appreciation to Dr. Takao Yamashita, Associate professor at DPRI, Kyoto University, for providing partially financial support to this research work.

REFERENCES

Asano, T. (1990). "Two-phase flow model on oscillatory sheet-flow." *Proceeding 22nd International Conference of Coastal Engineering*, ASCE, Delft, pp.2372-2384.

Horikawa, K., Watanabe, A., and Katori, S. (1982). "Sediment transport under sheet-flow condition." *Proceeding 18th International Conference of Coastal Engineering*, ASCE, Cape Town, pp.1335-1352.

Gotoh, H. and Sakai, T. (1997). "Numerical simulation of sheet-flow as granular materials." *Journal of Waterway, Port, Coastal, and Ocean Engineering*, ASCE, Vol. 123, No. 6, pp. 329-336.

Cundall, P.A. and Strack, O.D. (1979). "A discrete numerical model for granular assembles." *Geothechnique 29*, No. 1, pp. 47-65.

Yeganeh-Bakhtiary, A., Gotoh, H., and Sakai, T. (2000). "Numerical study of particle diameter effect on oscillatory sheet-flow transport with Movable Bed Simulator." *Annual Journal of Hydraulic Engineering*, JSCE, Vol. 44, pp.653-658.

Yeganeh-Bakhtiary, A. (1999). "Computational mechanics of bed-load transport at high bottom shear." Ph.D. dissertation, Kyoto University, Japan, pp. 94.

Tanaka, H. and Tua, A. (1993). "Wave-current friction law spanning all flow regimes." *Journal of Hydraulic, Coastal and Environmental Engineering*, No. 467/II-23, JSCE, pp. 93-102. (in Japanese)

Madsen, O.S. and Grant, W.D. (1976). "Quantitative description of sediment transport by waves." *Proceeding 15th International Conference of Coastal Engineering*, ASCE, New York, pp. 1093-1112.

Research Center for Disaster Environment, Disaster Prevention Research Inst., Kyoto University, Uji, Kyoto 611-0011, Japan. The correspondence may be directed via e-mail to the following

(E-mail : yeganeh@rcde.dpri.kyoto-u.ac.jp)

Department of Civil Engineering, Kyoto University, Kyoto 606-8501, Japan.